Journal of Power Sources 330 (2016) 261–272

Contents lists available at ScienceDirect

Journal of Power Sources

journal homepage: www.elsevier.com/locate/jpowsour

Cost-driven materials selection criteria for redox flow battery electrolytes

Rylan Dmello [a, b, 1], Jarrod D. Milshtein [a, c, 1], Fikile R. Brushett [a, d], Kyle C. Smith [a, b, *]

[a] Joint Center for Energy Storage Research, USA
[b] Department of Mechanical Science and Engineering and Computational Science and Engineering Program, University of Illinois at Urbana-Champaign, Urbana, IL, 61801, USA
[c] Department of Material Science and Engineering, Massachusetts Institute of Technology, Cambridge, MA, 02139, USA
[d] Department of Chemical Engineering, Massachusetts Institute of Technology, Cambridge, MA, 02139, USA

HIGHLIGHTS

- We develop a techno-economic model for redox flow battery (RFB) electrolytes.
- Electrolyte costs account for redox active material, salt, and solvent components.
- Reactor, balance-of-plant, and additional costs are considered.
- Design maps to build \$100 kWh^{-1} RFBs guide electrolyte materials selection.
- Multiple pathways to decreasing RFB electrolyte costs are proposed .

ARTICLE INFO

Article history:
Received 27 June 2016
Received in revised form
10 August 2016
Accepted 30 August 2016
Available online 13 September 2016

Keywords:
Redox flow battery
Electrolyte
Techno-economic model
Energy storage

ABSTRACT

Redox flow batteries show promise for grid-scale energy storage applications but are presently too expensive for widespread adoption. Electrolyte material costs constitute a sizeable fraction of the redox flow battery price. As such, this work develops a techno-economic model for redox flow batteries that accounts for redox-active material, salt, and solvent contributions to the electrolyte cost. Benchmark values for electrolyte constituent costs guide identification of design constraints. Nonaqueous battery design is sensitive to all electrolyte component costs, cell voltage, and area-specific resistance. Design challenges for nonaqueous batteries include minimizing salt content and dropping redox-active species concentration requirements. Aqueous battery design is sensitive to only redox-active material cost and cell voltage, due to low area-specific resistance and supporting electrolyte costs. Increasing cell voltage and decreasing redox-active material cost present major materials selection challenges for aqueous batteries. This work minimizes cost-constraining variables by mapping the battery design space with the techno-economic model, through which we highlight pathways towards low price and moderate concentration. Furthermore, the techno-economic model calculates quantitative iterations of battery designs to achieve the Department of Energy battery price target of \$100 per kWh and highlights cost cutting strategies to drive battery prices down further.

1. Introduction

Grid-scale energy storage technologies are becoming increasingly critical to promoting sustainable electricity generation. First, energy storage can alleviate the intermittency of renewable energy technologies (i.e., wind, solar), facilitating broad implementation [1]. Second, storage can also improve the cost-effectiveness of the existing fossil fuel infrastructure, decreasing electricity costs via load-leveling and price arbitrage operations [2]. Third, grid-scale storage can provide high value services such as back-up power, frequency regulation, and voltage support [2]. Redox flow batteries (RFBs) provide a promising technological pathway towards low-cost grid-scale energy storage devices due to decoupled capacity and power, long lifetimes, and facile thermal management [3–8].

* Corresponding author. University of Illinois at Urbana-Champaign, Department of Mechanical Science and Engineering, 105 S. Matthews Ave., Urbana, IL, USA.
E-mail address: kcsmith@illinois.edu (K.C. Smith).
[1] These authors contributed equally to this work.

http://dx.doi.org/10.1016/j.jpowsour.2016.08.129
0378-7753/

Current RFB prices, however, are too high for market penetration [9–11]. According to the Department of Energy (DOE) Office of Electricity Delivery and Energy Reliability, decreasing RFB system price to \$120 kWh^{-1} in the near term will enable widespread adoption for 4 h discharge grid-scale energy storage applications [3,9]. In comparison, the DOE's Advanced Research Projects Agency - Energy (ARPA-E) suggests a long-term energy storage battery price target of \$100 kWh^{-1} for 1 h of discharge [12]. In 2014, RFB prices exceeded \$500 kWh^{-1} [9,10]. Despite the existing high prices, recent work has established that both aqueous and nonaqueous RFBs can meet the desired \$100 kWh^{-1} battery price target by appropriately decreasing RFB reactor and materials costs contributions [9].

To achieve the price target, the price-to-energy ratios of aqueous and nonaqueous RFBs can drop by following different cost reduction pathways that optimize their fundamentally different reactor and materials characteristics [9]. Aqueous RFBs (AqRFBs) leverage inexpensive electrolytes, utilizing water as the solvent and typically a low-cost inorganic salt (e.g., H_2SO_4, KOH, and NaCl), while exhibiting high power density due to low cell resistance. The typical electrochemical stability window of water (less than 1.5 V), however, limits the maximum achievable AqRFB electrolyte energy density. In contrast, nonaqueous RFBs (NAqRFBs) employ nonaqueous solvents with wide electrochemical stability windows (3–4 V) and can thus enable electrolytes with greater energy density as compared to aqueous systems. Despite attractive voltage capabilities, NAqRFBs suffer from relatively expensive nonaqueous solvents (e.g., nitriles, glymes, and carbonates) and fluorinated salts (e.g., tetrafluoroborates, hexafluorophosphates, and bis(trifluoromethylsulfonyl)imides), as well as low power density due to low membrane conductivities. Considering the advantages and drawbacks of each system, AqRFB cost cutting efforts should maximize cell voltage, while NAqRFB design should decrease electrolyte cost and improve power density.

Redox-active materials for both families of RFBs require continued research and development for widespread adoption. Inorganic non-metallic (e.g., polysulfide-bromine) and transition metal (e.g., all-vanadium) redox-active materials have traditionally been at the forefront of AqRFB development, although metal coordination complexes have also been explored [7,13,14]. AqRFBs utilizing certain inorganic, non-metallic redox-active materials, such as bromine, have failed to penetrate the market due to their corrosive and toxic nature, making the practical design of flow fields, pumps, storage tanks, and pipes difficult [15]. Additionally, transition metal based AqRFBs have struggled to achieve the battery price targets due to the high cost and limited abundance of the redox-active material [6]. Early investigations into NAqRFBs employed metal coordination complexes as redox-active materials that suffer from low solubility, poor stability, or expensive precursors [16–19]. A significant portion of recent RFB progress beyond vanadium RFBs, arguably the current state-of-the-art systems, has aimed at identifying low-cost redox-active materials such as abundant inorganic species [20,21] and tailored organic molecules [22–34]. Organic redox-active molecules are particularly attractive for use in both aqueous and nonaqueous RFBs; organic molecules are comprised of earth abundant elements (e.g., hydrogen, carbon, oxygen, sulfur) and offer a broad design space, allowing for rational control of molecular weight, solubility, and redox potential by molecular functionalization [35].

RFB price relates to experimentally measurable chemical properties, electrochemical performance, and cost parameters that serve as critical inputs towards developing RFB cost projections via a techno-economic (TE) model. TE models have quantified the price performance of transportation [36,37] and grid-scale [9–11,38–40] energy storage devices. In 2014, Darling, Gallagher, and co-workers developed a comprehensive TE model (hereafter referred to as the DG model) to compare the price performance of aqueous and nonaqueous RFBs [9]. The DG model defined benchmark values for redox-active material concentration, molecular weight, cell voltage, and area-specific resistance (ASR), for both families of RFBs, to reduce battery price to \$100 kWh^{-1}. Although instrumental in elucidating future RFB prices, the DG model focused on a single set of benchmarks but did not explore alternative design iterations. A recent investigation into separator performance characteristics for RFBs considered the tradeoffs among cell voltage, ASR, and reactor cost [41], but no such sensitivity analysis has accounted for the relative cost contributions from the electrolyte constituent materials: solvent, salt, and redox-active compounds.

The present work addresses the lack of RFB design strategies by exploring the materials space mapped by an electrolyte-centric TE model, which identifies new RFB price reduction strategies. A detailed electrolyte cost model, explicitly accounting for redox-active species, salt, and solvent cost contributions, combined with the existing DG model, enables a sensitivity study of aqueous and nonaqueous RFB prices to various material and cost parameters. We explore the available RFB design space and investigate the sensitivity of both aqueous and nonaqueous RFBs to pertinent electrolyte constituent cost variables, cell voltage, and ASR. Further, maps of the available design space translate abstract price targets into quantitative performance targets, bridging the TE model to prototype guidelines. As such, this paper demonstrates tradeoffs in RFB constituent costs and performance to achieve a \$100 kWh^{-1} battery price. While previous modeling efforts have highlighted cost performance challenges with specific RFB chemistries (e.g. all-vanadium, zinc-bromine) [9–11,40], our analysis culminates in a set of design maps to aid in selecting materials for new RFB electrolytes. We also suggest research pathways to most easily achieve the near-term target battery price (\$100 kWh^{-1}) and lower. This electrolyte-centric analysis can guide future research efforts in the development and selection of new, promising materials for use in economically viable RFB prototypes.

2. Methodology

2.1. Model definitions

Redox flow battery price is defined as the RFB's future-state battery price P_0 (excluding power conditioning systems) per unit discharge energy E_d, delivered over a time t_d. The present TE model (which builds on the DG model [9]) separates RFB price into four major cost contributions from the reactor $C_{Reactor}$, electrolyte $C_{Electrolyte}$, additional $C_{Additional}$, and balance-of-plant (BOP) C_{BOP}:

$$\frac{P_0}{E_d} = C_{Reactor} + C_{Electrolyte} + C_{Additional} + C_{BOP} \quad (1)$$

Table 1 provides variable definitions for all cost equations, as well as benchmark values and units. Here, a series of design maps are presented in which certain model parameters vary. In addition, the supplementary information contains a MATLAB script that generates the design maps presented here. The parameters that do not vary in the design maps assume benchmark values (Table 1), unless otherwise explicitly stated. In these design maps, thin dotted black lines denote benchmark values from the original DG model.

This work builds on the reactor, additional, and BOP cost descriptions from the DG model. In the DG model [9], the reactor cost (in \$ kWh^{-1}) depends on the reactor cost per unit area c_a, which incorporates the costs associated with bi-polar plates, membranes, and seals; the cost of each reactor hardware component is detailed in Ref. [9]. Additionally, the reactor cost varies with area-specific

Table 1
Parameters utilized in the present techno-economic model. Benchmark values were obtained from the DG model [9]. *These material-specific targets were set in Ref. [9] as guidelines to achieve \$100 kWh^{-1} battery price, based on the values of the other parameters listed here.

Modeling parameter	Benchmark values	
	Nonaqueous	Aqueous
Reactor parameters		
Cost per unit area, c_a	\$107.5 m^{-2}	\$122.5 m^{-2}
Area-specific resistance, R	5.0 Ω-cm^{-2}	0.5 Ω-cm^{-2}
Open-Circuit Cell Voltage, U	3 V	1.5 V
Discharge time, t_d	5 h	5 h
System discharge efficiency, $\varepsilon_{sys,d}$	0.94	0.94
Voltage discharge efficiency, $\varepsilon_{v,d}$	0.916	0.916
Electrolyte parameters		
Round-trip coulombic efficiency, $\varepsilon_{q,rt}$	0.97	0.97
Stoichiometric coefficient, $s_\pm$	1	1
Allowable state-of-charge range, $\chi_\pm$	0.80	0.80
Actives molecular weight,* $M_\pm$	100 g mol^{-1}	100 g mol^{-1}
Actives cost per unit mass, $c_{m,\pm}$	\$5 kg^{-1}	\$5 kg^{-1}
Electrolyte cost per unit mass, $c_{me,\pm}$	\$5 kg^{-1}	\$0.1 kg^{-1}
Actives solubility,* $S_\pm$	1.0 kg kg^{-1}	0.2 kg kg^{-1}
Additional parameters		
Addition to price, c_{add}	\$112.5 kW^{-1}	\$87.5 kW^{-1}
Balance-of-plant cost, c_{bop}	\$102.5 kW^{-1}	\$102.5 kW^{-1}
DG model parameters		
Salt cost per unit mass, c_{salt}	\$20 kg^{-1}	–
Solvent cost per unit mass, $c_{solvent}$	\$2 kg^{-1}	\$0.1 kg^{-1}
Salt solubility,* $S_{salt,\pm}$	0.16 kg kg^{-1}	–
Mean molar salt ratio,* r_{avg}	0.20 mol mol^{-1}	–
Salt molecular weight, M_{salt}	100 g mol^{-1}	–
Mean actives molality,* b_{avg}	9.6 mol kg^{-1}	1.6 mol kg^{-1}

*These material-specific targets.

resistance R (including resistance contributions from the membrane, porous electrode, reaction kinetics, mass transfer, and electrical contacts), open-circuit cell voltage U, discharge voltage efficiency $\varepsilon_{v,d}$, system efficiency during discharge $\varepsilon_{sys,d}$ (including losses due to auxiliary equipment and pumping), and discharge time t_d:

$$C_{Reactor} = \frac{c_a R}{\varepsilon_{sys,d} U^2 \varepsilon_{v,d}(1-\varepsilon_{v,d}) t_d} \tag{2}$$

The balance-of-plant cost accounts for the ancillary equipment (such as pumps, controls, sensors, and pipes) required to build a working system, while the additional cost accounts for economic factors like depreciation, overhead, labor, and profit margin. A full discussion of these costs is provided in Ref. [9]. Importantly, this work considers a battery price, which excludes power conditioning systems (i.e., inverters) and installation costs [9]. The battery price is not to be confused with the system price, which does include power conditioning systems costs, as the system price may be the focus of other techno-economic modeling literature. The \$120 kWh^{-1} system price target used in the DG model is thus converted to a \$100 kWh^{-1} battery price target by excluding a power conditioning system that costs \$100 kW^{-1} for 5 h of discharge [42].

A new model is used for the electrolyte cost $C_{Electrolyte}$, in \$ kWh^{-1}, that incorporates cost contributions from individual materials in the electrolyte. Specifically, the costs from redox-active materials (used in the positive and negative electrolytes), supporting salt, and solvent are included explicitly. This electrolyte cost model captures the state of RFB materials as purchased from a chemical supplier. Further, the model normalizes the electrolyte materials costs by the total system energy, accounting for discharge efficiencies (as included in the reactor cost), round-trip coulombic efficiency $\varepsilon_{q,rt}$ (accounting for crossover and shunt current effects), open-circuit cell voltage, and depth-of-dischargeχ (the fraction of theoretical capacity accessed):

$$C_{Electrolyte} = \frac{1}{\varepsilon_{sys,d}\varepsilon_{q,rt}F\varepsilon_{v,d}U}\left(\frac{s_+M_+}{\chi_+ n_{e+}}c_{m,+} + \frac{s_-M_-}{\chi_- n_{e-}}c_{m,-} + 2r_{avg}M_{salt}c_{salt} + \frac{2}{b_{avg}}c_{solvent}\right) \tag{3}$$

The redox-active materials used in either the positive or negative electrolytes (denoted with '+' or '−' subscripts, respectively) store n_e electrons per s formula units of the particular redox-active species (also called the stoichiometric coefficient) that has molecular weight M with a cost per unit mass c_m. Equation (3) also accounts for the benefits of employing a cheaper salt or solvent in the RFB. Several variables specify the type and amount of salt employed, including the molar ratio of salt to redox-active species r (in moles of salt per mole of electrons stored), salt molecular weight M_{salt}, and the salt cost per unit mass c_{salt}. Solvent costs depend on the redox-active species concentration b (molality in units of moles of electrons transferred per kilogram of solvent) and the cost per unit mass of the solvent $c_{solvent}$. Note here that the molar ratio of salt to redox-active species and the redox-active species concentration appear as average values of the positive and negative electrolytes, assuming the symbols r_{avg} and b_{avg}, respectively [r_{avg} is an arithmetic mean with $r_{avg} = (r_+ + r_-)/2$, while b_{avg} is a harmonic mean with $b_{avg} = 2b_+b_-/(b_+ + b_-)$]. The Appendix relates these variables (r_{avg} and b_{avg}) to parameters from the DG model. This approach also accounts for the ion-transfer configuration of the RFB by modeling salt concentration variations. This capability enables comparison between rocking-chair and salt-splitting ion transfer configurations that are discussed in detail later (Section 3.2).

2.2. Material cost assumptions

The costs-per-unit-mass (\$ kg^{-1}) of redox-active materials, salts, and solvents in Table 1 assume future commodity-scale production and can vary depending on the choice of material. While these costs may appear optimistic, certain materials could achieve these values today; for example, the 2006 bulk price of acetonitrile, a typical NAqRFB solvent, was ~\$1.50 kg^{-1} [43]. Additionally, the two-fold decrease in lithium-ion battery electrolyte (1 mol L^{-1} salt + solvent) costs from \$40 kg^{-1} to \$18 kg^{-1} between 1999 and 2011 [37,44], suggests that other solvent and salt costs could realistically fall to the values listed in Table 1 over the next decade. Redox-active materials have an estimated future-state cost of \$5 kg^{-1}, however, tailored molecules can cost more if complicated synthetic procedures are required for manufacture [9]. Anthraquinone, a precursor to several other redox-active materials [22,23,45,46], has an estimated price of ~\$4.40 kg^{-1} [23,47]. Alternatively, inherently low-cost materials, such as those containing sulfur [48] or bromine [23] (the 2006 prices of S_8 and Br_2 were \$0.20 kg^{-1} and \$1.41 kg^{-1}, respectively [43]), can decrease future-state costs compared to tailored redox-active molecules. Furthermore, this study considers RFBs implementing a fluorinated ion-exchange membrane (i.e., Nafion) with an estimated future-state price of \$50 m^{-2} [9]. Our study does not consider how variations in membrane cost affects the available RFB design space because an excellent prior study (Ref. [40]) offers a comprehensive analysis of tradeoffs in membrane cost and performance.

3. Results and discussion

3.1. Mapping the RFB materials design space

We map the available materials design space for aqueous and

nonaqueous RFBs, within physical reason, to achieve a \$100 kWh^{-1} battery price. The analysis presented here remains within a design space commonly accessible by laboratory and industrial scale RFBs, even though extreme RFB electrolyte systems may be possible. To begin, this work explores the tradeoffs among cell voltage, redox-active material molecular weight, and redox-active material concentration for both aqueous and nonaqueous RFBs. Contours of constant concentration in Fig. 1a represent possible RFB designs with a \$100 kWh^{-1} price. Note that design maps throughout this work present molecular weight in units of "grams per mole of electrons" to accommodate active species that undergo multiple electron transfer events.

The thermodynamic dissociation potential of water is 1.23 V, but due to the sluggish kinetics of the hydrogen and oxygen evolution reactions on porous carbon electrodes, AqRFB cell voltages can typically reach 1.5 V (Fig. 1a, horizontal dashed line) [49]. In some exceptional battery systems, such as lead-acid and zinc-bromine, the water stability limit has exceeded 1.7 V [7,50]. RFBs with cell voltages greater than 2 V, however, will require the use of an aprotic nonaqueous solvent [9], which can easily exhibit electrochemical windows from 3 to 4 V [51]. Each concentration contour in Fig. 1a, for both aqueous and nonaqueous RFBs, demonstrates that as the molecular weight of the redox-active species increases, the required cell voltage to achieve \$100 kWh^{-1} also increases. Increasing molecular weight subsequently increases RFB price (in \$). Therefore, to offset higher redox-active material costs, the cell voltage must also rise, increasing the available system energy while simultaneously decreasing reactor and electrolyte costs (in \$ kWh^{-1}).

Notably for NAqRFBs, as the redox-active species molality decreases, either the cell voltage must increase or the molecular weight must decrease significantly to attain the target battery price, and this sensitivity results from higher solvent costs (\$2 kg^{-1}) than water. Redox-active species molality is directly proportional to electrolyte energy density, which subsequently defines the total available energy of the RFB. As redox-active material concentration decreases, the volume of electrolyte required to achieve a fixed system energy increases, and subsequently the amount and total cost of solvent also increases. Therefore, to achieve the target price, the battery energy must increase via a voltage increase, or the electrolyte cost must reduce by utilizing redox-active compounds with lower molecular weight. As a quantitative nonaqueous example, a 100 g mol^{-1} redox-active material at 20 mol kg^{-1} concentration requires a 2.8 V cell, but the same redox-active material requires a 4 V cell if the operating concentration drops to 2 mol kg^{-1}. Further, the NAqRFB design space is insensitive to molality changes at high redox-active material concentrations (greater than 20 mol kg^{-1}) because, in this regime, the solvent cost contribution approaches zero. Ultra-high NAqRFB concentrations (greater than 200 mol kg^{-1}) correspond to redox-active materials in near-neat form with minimal solvent content, and only liquid redox-active species can achieve such high concentrations. Liquid redox-active species are a new concept for NAqRFBs, demonstrated in Ref. [32]. Due to the decreasing solvent cost contribution at ultra-high redox-active material molality, the concentration contours for such redox-active liquids will closely match the 200 mol kg^{-1} contour, and thus, the NAqRFB feasible region in Fig. 1a, highlighted in green, exists above the 200 mol kg^{-1} contour. Additionally, Fig. 1a shows that a NAqRFB with a cell voltage less than 2 V will be financially infeasible.

In contrast to nonaqueous systems, AqRFB designs demonstrate negligible sensitivity across order of magnitude changes in redox-active species concentration (0.5–200 mol kg^{-1}). For AqRFBs, the supporting electrolyte cost contribution (\$0.1 kg^{-1}) is extremely low, and thereby, only the redox-active material molecular weight

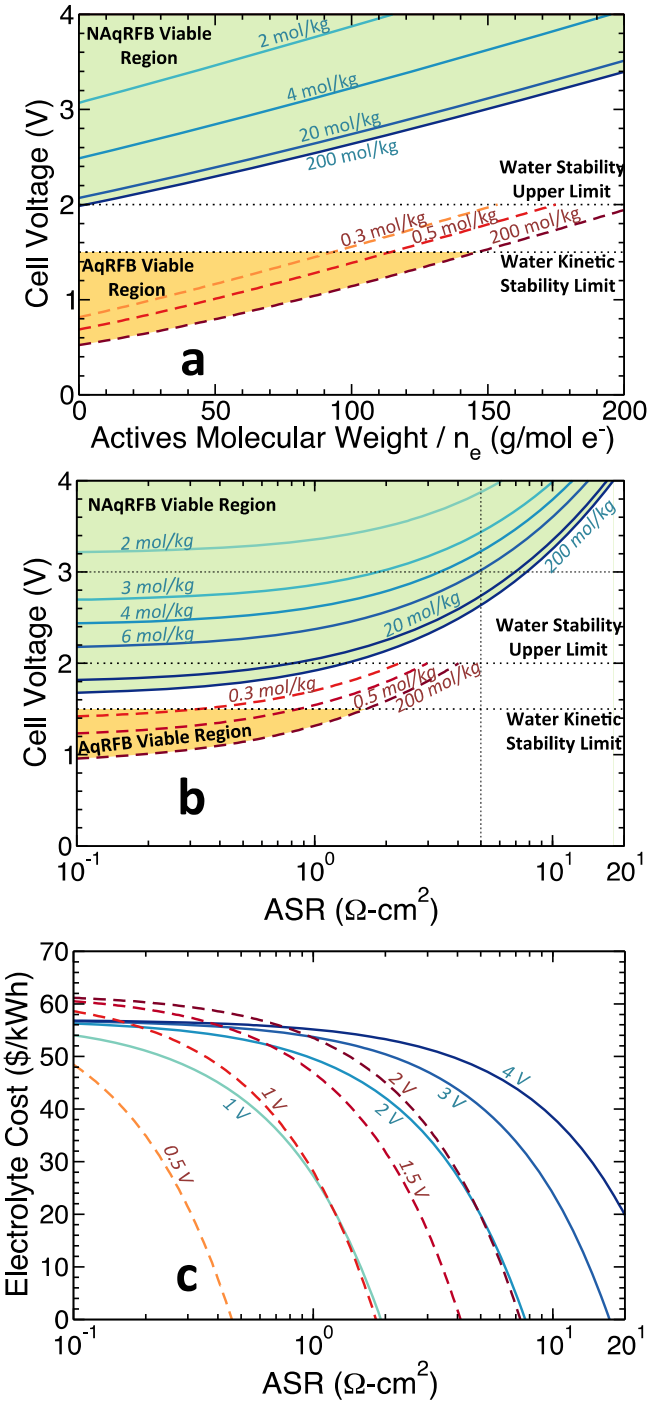

Fig. 1. Contours of constant redox-active species concentration for aqueous and nonaqueous RFBs as a function of cell voltage and **(a)** redox-active species molecular weight or **(b)** reactor ASR. Each contour achieves a battery price of \$100 kWh^{-1}. Contours above 2 V represent the NAqRFB feasible design space, while the shaded region below 1.5 V represents the AqRFB design space. Horizontal dotted lines at 1.5 V and 2 V denote the typical electrochemical stability window and upper stability limit of aqueous electrolytes, respectively. **(c)** Contours of constant cell voltage as a function of electrolyte cost ($C_{Electrolyte}$) and reactor ASR, where each contour achieves a battery price of \$100 kWh^{-1}. For all sub-figures, NAqRFB and AqRFB contours are represented as solid and dashed lines, respectively.

or cell voltage can substantially affect the design space. At extremely low concentrations (less than 0.5 mol kg^{-1}), however, AqRFBs require cell voltages greater than the electrochemical stability window of water to meet the cost targets. This voltage

requirement suggests a minimum concentration requirement of 0.5 mol kg^{-1} to maintain electrolyte stability and eliminate redox-active material molality as a cost constraint. The maximum stable cell voltage in aqueous solution and the minimum cell voltage required to recover electrolyte costs bound the AqRFB feasible design space (highlighted in yellow in Fig. 1a). In the regime of ultra-low redox-active species concentration (less than 0.5 mol kg^{-1}), AqRFBs may become sensitive to variations in other cost parameters such as pumping losses, cycle efficiencies, or tank sizes, which the design maps in Fig. 1a do not capture.

RFB design is also sensitive to reactor ASR. A recent study has shown that reactor ASR can drastically impact the required cell voltage for economically feasible RFBs [41], but changes in ASR can also affect the required redox-active material concentrations for NAqRFBs. Fig. 1b plots contours of constant concentration as a function of cell voltage and reactor ASR for both aqueous and nonaqueous RFBs. First, this analysis establishes that an upper bound on a maximum plausible ASR is approximately 20 Ω-cm^2; at this ASR value all NAqRFB designs would require cell voltages above 4.5 V, which would be difficult due to electrolyte breakdown [51]. Similarly, a maximum plausible ASR for AqRFBs is approximately 1.5 Ω-cm^2, beyond which an AqRFB would require a cell voltage exceeding 1.5 V, leading to imminent water dissociation. Considering the nonaqueous contours, Fig. 1b demonstrates a rapid decrease in required cell voltage or redox-active species concentration as ASR decreases in the range of 20 to 1 Ω-cm^2. The DG model recommended employing 3 V NAqRFB reactors with 5 Ω-cm^2 ASR and redox-active species concentration of 9.6 mol kg^{-1} [9], but a later study recommended decreasing the ASR of NAqRFBs down to 2.3 Ω-cm^2 [41], which could reduce the required redox-active species concentration to 4 mol kg^{-1}. For ASR values below 1 Ω-cm^2, NAqRFB cell voltage targets become relatively insensitive to further decreases in ASR. Again, due to low solvent costs for concentrations greater than 0.5 mol kg^{-1} AqRFB cell voltage and ASR requirements are less sensitive to redox-active species concentration, even over order of magnitude changes. AqRFBs with concentrations less than 0.5 mol kg^{-1} are infeasible at \$100 kWh^{-1} due to high cell voltage requirements that extend beyond the stability window of aqueous electrolytes. Fig. 1b, however, also demonstrates that decreasing ASR for aqueous systems below 1 Ω-cm^2 could decrease cell voltage requirements down to under 1.2 V, broadening the number of viable redox-active materials for use in AqRFBs. Due to the inherent constraint of the narrow AqRFB electrochemical window, small improvements in ASR could lead to a critical decrease in required AqRFB cell voltage.

We directly illustrate the relationship among reactor ASR and electrolyte cost ($C_{Electrolyte}$) with a series of concave-down cell voltage contours in Fig. 1c. Generally, as ASR decreases, electrolytes that are more expensive enter the available design space, but as ASR increases, electrolyte cost must decrease to compensate for the associated rise in reactor cost. In addition, higher cell voltage permits both higher electrolyte cost and ASR, as the cell voltage is a critical parameter in determining both the reactor and electrolyte costs. For example, the higher cell voltages possible in NAqRFBs can offset the higher costs and ASR values associated with nonaqueous electrolytes. Given the electrochemical stability windows of typical aqueous and nonaqueous electrolytes, Fig. 1c reaffirms our suggested bounds on reactor ASR for both RFB families. While Fig. 1c demonstrates interesting tradeoffs in reactor and electrolyte cost contributions, the total electrolyte cost is difficult to decompose into price optimization pathways for individual electrolyte components.

Considering only cell voltage, ASR, redox-active material molecular weight, and redox-active material concentration as design parameters, the variability of battery price is evident for both aqueous and nonaqueous RFBs. The difference in design sensitivity between the two systems leads to fundamentally different challenges in materials selection at fixed battery price. Recent reports have already demonstrated NAqRFBs with cell voltages greater than 2 V [52,53], and low molecular weights less than 200 g mol^{-1} [28,33,54]. These early advances suggest that the cell voltage and molecular weight benchmarks of 3 V and 100 g mol^{-1} may be possible in the future. The corresponding redox-active material concentration target of 9.6 mol kg^{-1} (~4–5 mol L^{-1}, assuming specific electrolyte volume of 1 L kg^{-1} and solvent mass fraction of ~0.4–0.5) for NAqRFBs, however, would be difficult to achieve experimentally. State-of-the-art tailored organic redox-active materials developed by Sevov et al. and Huang et al. had solubility limits less than 2 mol L^{-1} [33,54]. Decreasing the required redox-active material concentration becomes a critical design optimization pathway for economically viable NAqRFBs. Since AqRFB design is relatively insensitive to solvent costs, AqRFBs can operate in a cost effective manner even at low redox-active material concentrations, but viable AqRFBs will require cell voltages in the range of 1.2–1.5 V and ASR values below 1.5 Ω-cm^2. While many AqRFBs, including vanadium systems, demonstrate cell voltages exceeding 1 V, low-cost redox-active species that maximize use of aqueous electrochemical stability windows are essential to achieve a low battery price.

3.2. Nonaqueous RFB design optimization

To enable NAqRFBs with sufficiently high cell voltages, positive electrolyte materials must have relatively high redox potentials, while negative electrolyte materials must have relatively low redox potentials. The difference between the redox potentials of the positive and negative redox-active materials will define the total NAqRFB cell voltage, and thus, the positive and negative electrolytes each require unique materials selection criteria. Fig. 2 quantifies required changes in individual electrolyte material redox potential as a function of molecular weight for various redox-active material concentrations.

To allow such an analysis, Fig. 2 pairs positive electrolyte materials with a benchmark negative electrolyte material that has the same molecular weight per electron transferred as the positive active material of interest, but with a redox potential of 1 V vs. Li/Li^+. Conversely, the analysis pairs negative electrolyte materials

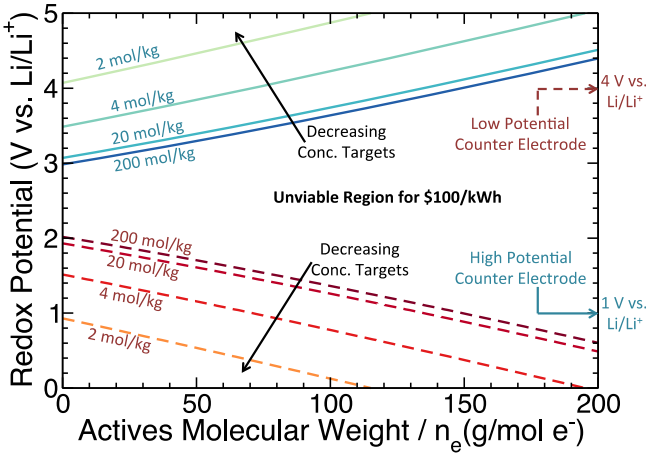

Fig. 2. Contours of constant of redox-active species concentration, as a function of redox-active species molecular weight and redox potential, for NAqRFBs, that achieve a battery price of \$100 kWh^{-1}. Solid contours correspond to positive redox-active materials, and dashed contours correspond to negative redox-active materials. The right hand *y*-axis displays the benchmark counter-electrode potentials.

with a benchmark positive electrolyte material, again, with the same molecular weight per electron transferred as the negative active material of interest, but exhibiting a redox potential of 4 V vs. Li/Li^+. In Fig. 2 contours with $E^o > 3$ V vs. Li/Li^+ (solid) correspond to positive electrolyte materials, while contours with $E^o < 2$ V vs. Li/Li^+ (dashed) correspond to negative electrolyte materials. The positive and negative electrolyte contours exhibit complementary trends to the cell voltage contours in Fig. 1a; specifically, increasing redox-active material molecular weight requires a more extreme redox potential to achieve \$100 kWh^{-1}. In addition, as redox-active material concentration decreases for a fixed molecular weight, the target system design requires more extreme redox potentials. The region between the positive and negative electrolyte contours represents an infeasible region for redox-active material use in a NAqRFB. Redox potentials in this region are too moderate to enable high enough cell voltages to offset the associated reactor and electrolyte costs. Fig. 2 ultimately demonstrates that by identifying redox-active materials with more extreme redox potentials, or by decreasing redox-active material molecular weight, nonaqueous electrolytes with lower concentrations of redox-active materials become cost effective.

Until now, the TE analysis has only considered the redox-active material and solvent cost contributions to NAqRFB electrolytes, but salt costs (\$20 kg^{-1}) will be higher than either redox-active materials (\$5 kg^{-1}) or solvent costs (\$2 kg^{-1}) due to the high cost associated with fluorinated anions. Fig. 3a demonstrates the relationship among salt cost, salt molecular weight, and redox-active species concentration. For each contour of constant concentration, as salt cost increases, the salt molecular weight must decrease, and vice versa. This simple trend arises to maintain the same overall cost of salt (in \$) for a fixed redox-active material concentration. The DG model estimated a salt cost of \$20 kg^{-1}, but the variation in cost among lithium salts [55], suggests that cheaper materials, below \$20 kg^{-1}, could be used for NAqRFBs. Salt candidate searches should consider new lithium-ion battery salts, such as chelated phosphates, borates, imides, and heterocyclic amines [56], as a possible pathway to decrease materials cost. Identifying cheaper or lower molecular weight salts can minimize redox-active species concentration requirements for NAqRFBs.

Aside from identifying overall cheaper salts, carefully selecting NAqRFB redox reactions can minimize the total salt cost contribution to the electrolyte cost. Consider that the salt plays three roles in a NAqRFB electrolyte. First, dissolved salt imparts conductivity on an otherwise insulating nonaqueous solvent, allowing for ionic conduction through the pore phase of a porous electrode. Second, the salt ions act as ionic charge carriers through the membrane of the RFB, which is a key attribute of any electrochemical cell. Third, the salt will serve to maintain electroneutrality in the bulk electrolyte throughout the entire RFB while redox-active materials undergo reduction or oxidation. Importantly, the requirement of bulk electroneutrality can lead to unnecessarily high concentrations of salt and subsequently unnecessarily high salt costs if the charges on the redox-active materials are dissimilar [57].

Equations (4)–(6) show three distinct reaction schemes for RFBs (assuming one electron stored for each redox-active species), where A is the positive electrolyte redox-active material and B is the negative electrolyte redox-active material:

$$A + B \leftrightarrow A^+ + B^- \quad (4)$$

$$A^{(n+1)-} + B^{n-} \leftrightarrow A^{n-} + B^{(n+1)-} \quad (5)$$

$$A^{n+} + B^{(n+1)+} \leftrightarrow A^{(n+1)+} + B^{n+} \quad (6)$$

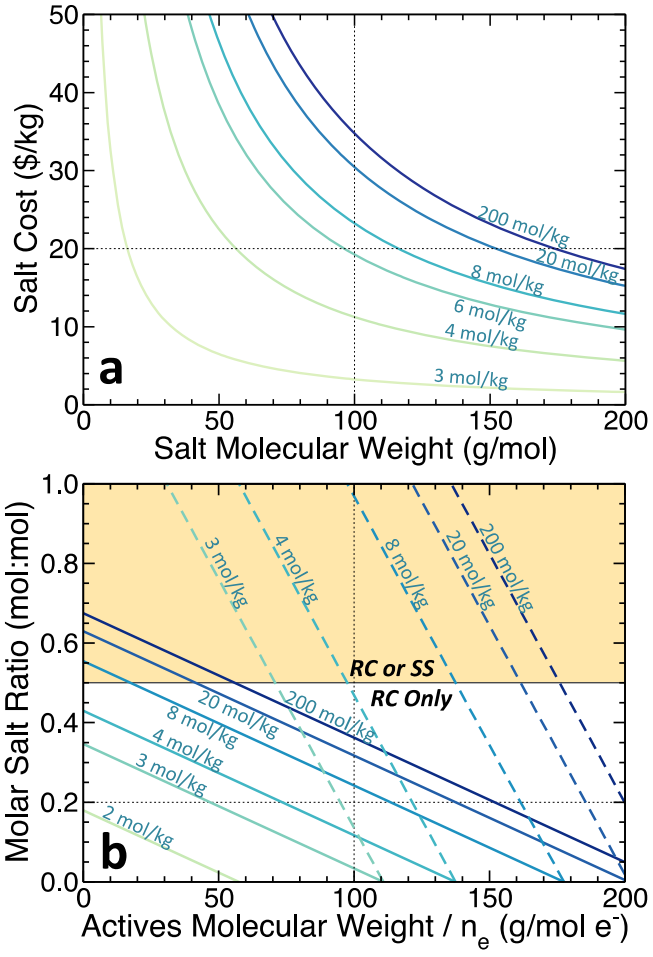

Fig. 3. **(a)** Contours of constant redox-active species concentration as a function of salt cost and salt molecular weight for NAqRFBs. Each contour achieves the target \$100 kWh^{-1} battery price. **(b)** Contours of constant redox-active species concentration for NAqRFBs, as a function of average molar salt ratio and redox-active species molecular weight, which satisfy the \$100 kWh^{-1} battery price target. The bottom half of the design space ($r_{avg} < 0.5$) is only accessible by rocking-chair (RC) configuration RFBs, while the upper half ($r_{avg} \geq 0.5$) is available to either rocking-chair or salt-splitting (SS) cells. The shaded upper half region represents the viable design space for salt-splitting cells. Solid contours correspond to a salt cost of \$20 kg^{-1}, and dashed contours correspond to a salt cost of \$5 kg^{-1}. Dotted black lines denote benchmark values.

The first reaction (Eq. (4)) represents a salt-splitting configuration, where both redox-active materials begin as neutral species at 0% state of charge (SOC), but then A oxidizes to a cation and B reduces to an anion at 100% SOC. The use of dissimilar charged species at 100% SOC will drive salt cations to the negative electrolyte, while salt anions migrate to the positive electrolyte. Thus, the salt-splitting configuration requires a minimum of one salt molecule for every two redox-active molecules (i.e., including redox-active molecules in both the positive and negative electrolytes) to maintain electroneutrality across all SOCs. This condition restricts the molar salt ratio r_{avg} to values in excess of 50% for salt-splitting configurations. Many NAqRFBs presented in literature exhibit a salt-splitting configuration due to the wider availability of stable redox-active materials in neutral state [24–26,34,53]. In contrast, Eqs. (5) and (6) (where n is an integer greater than or equal to zero) represent a special case of rocking-chair configuration RFBs, also sometimes referred to as common-ion exchange RFBs [57]. In these systems, either a single cation (Eq. (5)) or a single anion (Eq. (6)) transfers across the membrane to maintain electroneutrality [57], resembling ion transfer in a traditional lithium-ion battery [58]. By

utilizing a single ion to facilitate charge transfer across the membrane and redox-active materials that maintain the same sign of charge (cation or anion) across all SOCs, rocking-chair RFBs do not require any salt to charge balance (i.e., $r_{avg} \geq 0$); the salt in a rocking-chair cell merely imparts ionic conductivity to the electrolyte and membrane. Rocking-chair RFBs require that at least one of the redox-active materials be ionic at 0% SOC, and this ionic redox-active material must pair with an associating counter ion [57]. While uncommon in recent literature, some reports demonstrate rocking-chair NAqRFBs [16,17,59–62].

Switching NAqRFB configuration towards rocking-chair systems will allow for decreasing salt concentrations, which can dramatically widen the NAqRFB design space by eliminating costly salt from the system. Fig. 3b relates the required redox-active species concentration to molar salt ratio and redox-active species molecular weight for various NAqRFB designs, assuming two different salt costs of \$5 kg^{-1} (dashed lines) and \$20 kg^{-1} (solid lines). Each iso-concentration contour exhibits a near linear decrease of molar salt ratio with increasing redox-active species molecular weight; to offset higher total redox-active material costs, the total salt cost, and thereby salt concentration, must decrease. When constructing a RFB in rocking-chair configuration, redox-active species in at least one of the electrolytes must be an ion. Such a material would be purchased with an associated counter ion that increases the molecular weight of the redox-active material (relative to its molecular weight as a neutral species). Thus, Fig. 3b can assist in balancing molecular weight with the amount of dissolved salt in the NAqRFB. Further, as the redox-active species concentration decreases, either the molar salt ratio or redox-active species molecular weight must decrease to offset higher solvent costs. In Fig. 3b, values of $r_{avg} < 0.5$ represent a design space that is only accessible by employing a rocking-chair NAqRFB design. The DG model assumed 1 mol L^{-1} salt concentration for NAqRFB electrolytes [9], which, through our analysis, corresponds to $r_{avg} = 0.20$. As we show here, this salt ratio is only compatible with a rocking-chair configuration NAqRFB, where fewer moles of salt are present in the electrolyte than moles of redox-active material. For a salt cost of \$20 kg^{-1}, salt-splitting cells are financially infeasible, unless the redox-active materials exhibit unrealistically low molecular weights (<50 g mol^{-1}) and high concentrations (>8 mol kg^{-1}). The salt-splitting design space, however, does become accessible for a salt cost of \$5 kg^{-1}. As such, NAqRFB design is sensitive to salt cost and salt concentration due to the anticipated high costs of NAqRFB salts relative to redox-active material and solvent costs, and, by carefully minimizing salt cost and concentration, lower redox-active species concentrations, under 4 mol kg^{-1}, become feasible.

3.3. Aqueous RFB design optimization

While NAqRFB price is sensitive to all constituent electrolyte material costs, cell voltage, and ASR, the cost contributions of salt and solvent in AqRFBs are small. Consequently, the battery price of AqRFBs is sensitive neither to redox-active species concentration nor cell configuration (i.e., either rocking-chair or salt-splitting). These insensitivities stem from the extremely low-cost supporting electrolytes afforded in aqueous systems. Therefore, AqRFB design optimization focuses on varying cell voltage, ASR, redox-active material molecular weight, and redox-active material cost per unit mass to achieve \$100 kWh^{-1}.

Aqueous redox-active materials require sufficiently extreme redox potentials (high potential for positive redox-active materials, low potential for negative redox-active materials) to construct cells with voltages that are high enough to achieve the target battery price, but the redox potentials of the redox-active species are also constrained by the electrochemical stability window of aqueous electrolytes. Figure 4 demonstrates the difficulty in identifying viable redox-active species for AqRFBs, by plotting contours of constant redox-active material concentration in the space of redox potential (vs. the Reversible Hydrogen Electrode (RHE)) and molecular weight. Here, the respective benchmark counter-electrodes at −0.1 V and 1.4 V vs. RHE are paired with positive and negative electrolyte materials of interest for AqRFBs in a manner similar to NAqRFBs in Fig. 2. As a quantitative example, a positive electrolyte material with a molecular weight of 100 g mol^{-1} must have a redox potential in the range 1.1 V < E^o < 1.4 V vs. RHE; this is a narrow 300 mV design space to investigate, eliminating many possible redox-active material candidates. If the redox-active species molecular weight increases beyond 100 g mol^{-1}, the available design space shrinks even further. Selecting redox-active materials that enable AqRFBs with cell voltages >1.1 V is of paramount importance.

Beyond individual redox-active species selection, tradeoffs between reactor and electrolyte cost contributions can broaden the available design space. Figure 5a shows the relationship among required cell voltage, ASR, and redox-active material molecular weight to achieve a battery price of \$100 kWh^{-1}. As previously shown in Fig. 1b, the ASR must be under 1.5 Ω-cm^2 if the redox-active material exhibits a reasonable molecular weight (~100 g mol^{-1}), and any molecular weight greater than 150 g mol^{-1} would require unrealistically high cell voltages for aqueous systems. If extremely low molecular weight redox-active materials (<50 g mol^{-1}) were available, the maximum allowable ASR could increase to 4 Ω-cm^2, but such low weights would require molecular simplicity similar to that of an ethanol molecule (46 g mol^{-1}). Such simple species are likely to undergo only chemically irreversible redox events. Additionally, drastically decreasing cell ASR to an ultra-low value of 0.1 Ω-cm^2 affords only a 20% decrease in cell voltage target. The practical difficulties in decreasing molecular weight and ASR suggest that these are unviable design pathways towards decreasing AqRFB cell voltage requirements. Thus, we conclude that the most viable pathways towards achieving the desired battery price for AqRFBs are either by minimizing redox-active material cost (\$ kg^{-1}) or by maximizing cell voltage.

As an illustration, Fig. 5b reveals how decreasing redox-active material cost balances variations in cell voltage to achieve \$100 kWh^{-1}. The benchmark value for redox-active material cost of \$5 kg^{-1} corresponds to a required cell voltage of 1.2 V, but employing a redox-active material cost of \$1 kg^{-1} reduces the cell

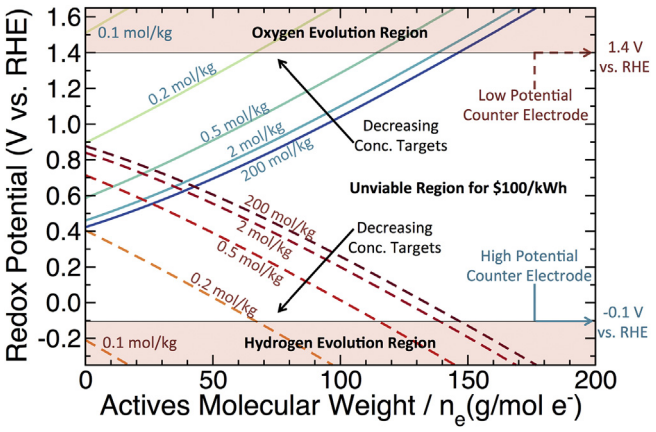

Fig. 4. Contours of constant redox-active species concentration for AqRFBs, as a function of redox-active species molecular weight and redox potential, which achieve a battery price of \$100 kWh^{-1}. Solid contours correspond to positive electrode materials, and dashed contours correspond to negative electrode materials. The right hand *y*-axis displays the benchmark counter-electrode potentials.

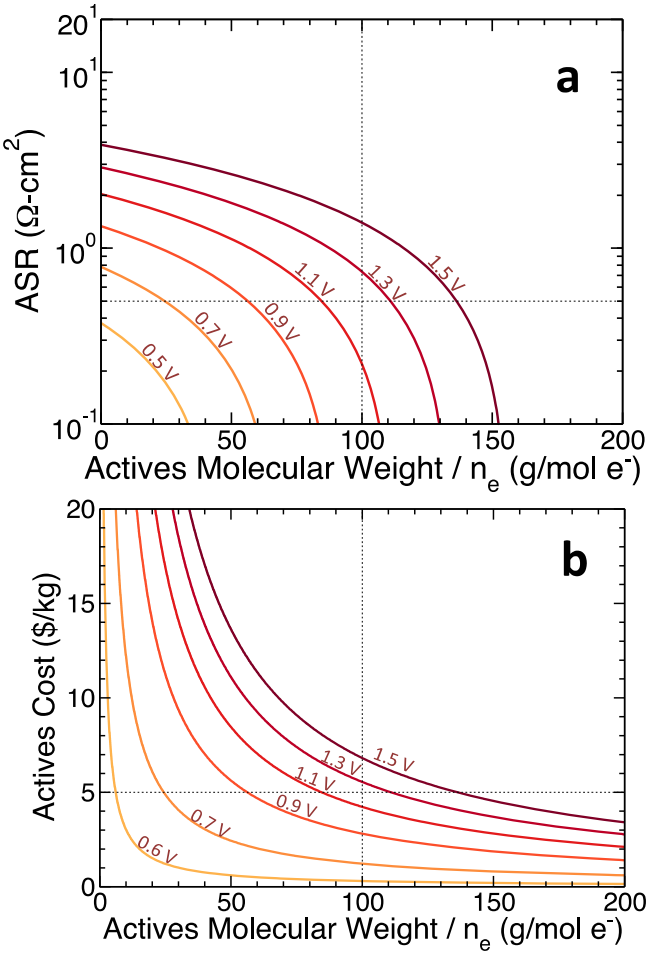

Fig. 5. **(a)** Contours of constant cell voltage for AqRFBs, as a function of ASR and redox-active species molecular weight, which achieve a battery price of \$100 kWh^{-1}. **(b)** Contours of constant cell voltage for AqRFBs, as a function of redox-active species cost and molecular weight, which achieve a \$100 kWh^{-1} battery price. Dotted lines illustrate the benchmark values for an AqRFB.

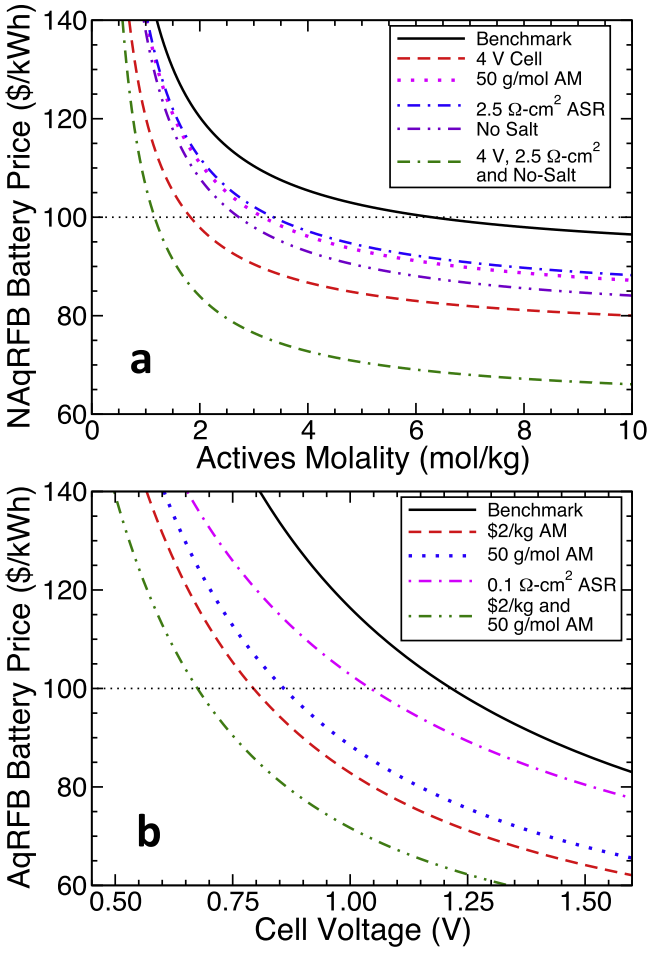

Fig. 6. Suggested design pathways that minimize cost and expand the design space for critical design constraints for **(a)** NAqRFBs and **(b)** AqRFBs. The horizontal dashed line represents the \$100 kWh^{-1} battery price target. "Active Material" is abbreviated as AM in the legend.

voltage requirement as low as 0.7 V. We can thus identify redox-active material cost and cell voltage as the two most critical parameters in building economically viable AqRFBs.

4. Recommended RFB design pathways

The RFB materials selection maps presented in this work are powerful tools for quantifying the tradeoffs among various electrolyte material costs, cell voltage, and ASR, but extracting design rules from them can be overwhelming due to the large number of variables and wide range of values each variable may assume. To this end, we propose generalized RFB design guidelines aimed at assisting in electrolyte materials selection. The DG model began such a design process by suggesting single iterations of aqueous and nonaqueous RFB designs [9], but the plethora of available iterations outlined in this work hints that even more realistic and cost effective pathways may exist.

4.1. Nonaqueous RFB design pathways

As NAqRFB price is sensitive to electrolyte components, cell voltage, and ASR, many possible NAqRFB design iterations become available, and Fig. 6a outlines new design pathways, showing NAqRFB price as a function of redox-active species concentration for various design improvements over the DG model baseline. As observed in Fig. 6a, the DG model suggestions achieve the target \$100 kWh^{-1} battery price at challenging redox-active material concentrations (greater than 6 mol kg^{-1}) [9]. As a first possible design improvement, decreasing cell ASR down to 2.5 Ω-cm^2, a value recommended by a study of RFB area-specific resistance [41], affords a small decrease in battery price. Experimental studies of membrane performance demonstrate significant variability in preventing crossover and facilitating ion transfer [53,59,63,64]. Finding a membrane (or separator) for NAqRFBs with high selectivity and that performs at high currents is one major materials challenge to overcome [41]. Beyond the ohmic contribution to NAqRFB resistance, the transport capabilities of nonaqueous solvents in porous electrodes present a challenge. Due to the high viscosity of some NAqRFB electrolytes [65,66], resistance due to pore-scale mass transfer of redox-active species and ionic conduction through the electrode thickness could possibly be similar in magnitude to the separator/membrane resistance.

Employing extremely cheap or lightweight redox-active materials (~50 g mol^{-1}) could afford similar cost savings as the decrease in ASR described above (Fig. 6a), but, as previously mentioned, such light species are unlikely to be electrochemically reversible compounds. Identifying redox-active materials with molecular weights between 100 and 200 g mol^{-1}, which participate in multiple electron transfer events, such as those developed by Sevov et al. [54],

Table 2
Alternative NAqRFB and AqRFB design iterations that decrease redox-active material molality targets and cell voltage targets by changing other parameters (bolded). All cells shown achieve the \$100 kWh^{-1} price target.

Nonaqueous RFB					
Cell type	Cell voltage (V)	Actives Mol. Weight (g mol^{-1})	ASR (Ω-cm^2)	Salt ratio	Actives Molality (mol kg^{-1})
1. Benchmark	3	100	5	0.20	6.3
2. High Cell Voltage	**4**	100	5	0.20	1.8
3. Low Actives Molecular Weight	3	**50**	5	0.20	3.1
4. Low ASR	3	100	**2.5**	0.20	3.3
5. No Salt	3	100	5	**0**	2.7
6. High Cell Voltage, Low ASR, and No Salt	**4**	100	**2.5**	**0**	1.1

Aqueous RFB				
Cell type	Actives cost (\$ kg^{-1})	Actives Mol. Weight (g mol^{-1})	ASR (Ω-cm^2)	Cell voltage (V)
1. Benchmark	5	100	0.5	1.21
2. Low Actives Cost	**2**	100	0.5	0.79
3. Low Actives Molecular Weight	5	**50**	0.5	0.85
4. Low ASR	5	100	**0.1**	1.04
5. Low Actives Cost and Low Actives Molecular Weight	**2**	**50**	0.5	0.67

may present a viable cost-cutting pathway. Recent reports demonstrate metal coordination complexes exhibiting up to six redox events [60], but these compounds have very high molecular weights and offer only moderate redox potentials. Two electron (or more) transfer materials could decrease the equivalent weight (molecular weight normalized by number of electrons transferred) into the range of 50–100 g mol^{-1}.

Salt cost contributions have a large effect on NAqRFB system design options. In particular, Fig. 6a shows that the battery price of a NAqRFB with no salt is lower than the benchmark value by approximately \$10 kWh^{-1} for moderately high redox-active species concentration. Removing salt from NAqRFBs may actually be a practical option in decreasing battery price by employing ionic liquid solvents, deep eutectic melts [67,68], or all ionic redox-active materials. First, ionic liquid solvents can cost 5–20 times more than molecular solvents [69], but the cost decrease afforded by removing salt from the electrolyte could make certain ionic liquid solvents viable. Additionally, we recommend investigation into RFBs utilizing protic ionic liquids (e.g., methanesulfonic acid, triethylammonium hydrogen sulfate), which can exhibit costs [70] and electrochemical windows [71] in between those of water and molecular nonaqueous solvents. Second, deep eutectic melts employing a redox-active material (e.g., $FeCl_3$ [67]) and a miscible host (e.g., choline chloride [67,68]) may offer an attractive pathway to no-salt NAqRFBs with moderate redox-active species concentrations (approximately 3.6 mol kg^{-1}) [67]. Third, redox-active materials that maintain ionic nature throughout all SOCs (e.g., metal centered bypiridines [16–18,62]) could serve as redox-active charge carriers, also eliminating the need for a supporting salt. Identifying any such multi-function materials that assume two or more roles in the electrolyte (i.e., redox-active, charge carrier, solvation) could enable large cost savings for NAqRFBs.

One final recommendation towards decreasing NAqRFB price is simply to increase cell voltage to approximately 4 V, which yields the most drastic decrease in NAqRFB price considered. Nonaqueous electrolytes offering a 4 V electrochemical window could easily enable low concentration batteries with a low price. Cell voltage affects the total battery price so dramatically because increased voltage decreases both the electrolyte (Eq. (3)) *and* reactor (Eq. (2)) cost contributions simultaneously. Molecular nonaqueous solvents, such as propylene carbonate, exhibit large electrochemical windows allowing for 4 V electrochemical cells [51], and some work has demonstrated fluorinated organic solvents designed for use in 5 V lithium-ion batteries [72]. Additionally, soluble redox-active compounds have proven redox potentials as high as 4.6 V vs. Li/Li$^+$ [73], but stable, soluble redox-active compounds with potentials less than 1.5 V vs. Li/Li$^+$ are not available. Identifying redox-active species with low redox potentials for use in the negative electrolyte of a NAqRFB remains a major materials design challenge [35,54].

To complement the price minimization trends offered in Fig. 6a, Table 2 presents quantitative design iterations for NAqRFBs to achieve a \$100 kWh^{-1} battery price, providing tangible performance guidelines for materials selection. By pushing NAqRFB design to incorporate any one of the proposed cost cutting pathways (high voltage, low ASR, low salt concentration, or low redox-active material weight), redox-active material concentration requirements shrink by more than 50% of the DG model benchmark (9.6 mol kg^{-1}). Driving redox-active material concentration below 1 mol kg^{-1} is unlikely, as demonstrated by the divergence to infinity of every price curve in Fig. 6a at low values of redox-active species molality. If a NAqRFB can leverage all of the cost cutting pathways presented here, the battery price could easily drop below \$100 kWh^{-1} for redox-active species concentrations greater than 2 mol kg^{-1}.

4.2. Aqueous RFB design pathways

While this work presents many pathways towards low-cost NAqRFBs, design optimization pathways for AqRFBs are substantially more limited since AqRFBs are only sensitive to variations in cell voltage, ASR, and redox-active species cost. Fig. 6b displays AqRFB prices as a function of cell voltage for a limited number of possible cell improvement pathways. In addition, Table 2 also presents quantitative iterations of AqRFB designs that achieve \$100 kWh^{-1}. Much like the NAqRFB, employing redox-active materials with low molecular weights only affords a small decrease in battery price, and, as previously described, synthesizing redox-active species with molecular weight much below 100 g mol^{-1} is unlikely. Decreasing redox-active species cost, however, can provide the most drastic savings, alleviating cell voltage requirements or driving battery prices down below \$100 kWh^{-1}; low-cost tailored organic [22,23,29,30,45,74] or abundant inorganic [20] materials could offer redox-active species costs under \$5 kg^{-1}. If an AqRFB exploits both low redox-active material cost and high cell voltage (approaching the stability limit of 1.5 V), AqRFB price could drop below \$100 kWh^{-1}.

5. Conclusions

In this work, we present a detailed electrolyte cost model, which explicitly accounts for redox-active material, salt, and solvent contributions to RFB price, as an adaptation to and an extension of

prior work by Darling, Gallagher, and co-workers [9]. This techno-economic model explores the available design space for both aqueous and nonaqueous RFBs by considering variations in electrolyte cost parameters, cell voltage, and reactor ASR, as well as identifying critical cost constraining variables for RFBs. In a broad sense, this analysis first defines lower bounds on cell voltage requirements of 1.1 V and 2.0 V for aqueous and nonaqueous RFBs, respectively, to obtain a \$100 kWh^{-1} battery price. Additionally, upper bounds on reactor ASR for aqueous and nonaqueous RFBs are 1.5 Ω-cm^2 and 20 Ω-cm^2, respectively.

NAqRFBs are sensitive to every cost parameter considered in this analysis due to comparable cost contributions from the electrolyte components and reactor, but the largest potential cost savings for NAqRFBs come from either increasing cell voltage above 3 V or minimizing the amount of supporting salt. We propose identifying materials that provide two or more functions in the electrolyte (i.e., charge balancing, electroactivity, solubilization, and ionic conductivity), which remove the need for a true salt or solvent and could enable much more cost effective nonaqueous electrolytes. In comparison, NAqRFB cost cutting by decreasing cell ASR below 5 Ω-cm^2 or reducing redox-active material molecular weight below 100 g mol^{-1} only affords small gains. These same techniques can also reduce the required NAqRFB redox-active species concentration to reasonably low values of 2–4 mol kg^{-1}, which are near experimental realization. Unlike nonaqueous systems, AqRFBs only exhibited large cost sensitivities to cell voltage and redox-active material cost. Identifying low-cost (less than \$5 kg^{-1}) redox-active materials that enable a cell voltage in the range of 1.1–1.5 V is the most promising pathway towards economically viable AqRFBs.

Another application of the present cost-driven materials selection approach is to curate databases of redox-active molecules compiled either experimentally [75–78] or computationally [79]. By comparing the performance of a real, new RFB electrolyte material with these design maps, experimentalists can quickly determine if the new electrolyte chemistry could achieve the \$100 kWh^{-1} price target. Further, computational data sieving is already underway, in conjunction with the Materials Project, which stores electrochemical data for thousands of *ab initio* predicted redox-active molecules as candidates for RFB electrolytes [79]. Accordingly, the present model has been implemented as an interactive online tool within the Materials Project, called the RFB Dashboard [80]. The RFB Dashboard filters redox-active molecules with suitable redox potentials and molecular weights to build a \$100 kWh^{-1} aqueous or nonaqueous RFB by using the design maps presented here (see Figs. 2 and 3). This online tool also allows users to adjust model input parameters to assess impact on materials selection, as well as to accommodate future changes to material cost factors and RFB performance parameters.

Beyond the immediate application to RFB materials selection, this analysis presents a framework for cost-conscious research efforts. The design maps translate system-level price and performance metrics to quantitative guidelines for materials properties and performance. Bridging the gap between abstract cost models and focused experimental research will enable rapid transition of new materials into economically viable prototypes. Design maps also highlight promising regions of design space that may be underexplored in the contemporary literature. We hope that this methodology will apply to other systems where cost is a major inhibitor to success by creating tangible experimental targets from detailed techno-economic modeling.

Acknowledgements

This work was supported as part of the Joint Center for Energy Storage Research, an Energy Innovation Hub funded by the U.S. Department of Energy, Office of Science, Basic Energy Sciences. Jarrod Milshtein also acknowledges financial support from the National Science Foundation Graduate Research Fellowship Program (DGE 1256260). The authors would like to thank the JCESR Flow Chemistry Sprint team for their continued input and support, including Dr. Xiaoliang Wei, Dr. Rama Vemuri, Dr. Wentao Duan, Dr. Levi Thompson, Dr. Krista Hawthorne, Dr. Tanya Breault, and Sydney Laramie. We especially thank Dr. Robert Darling and Dr. Kevin Gallagher for their valuable input regarding this project. Furthermore, we thank members of the Brushett Group at MIT and the Smith Group at UIUC for constructive feedback throughout the project.

Appendix

The present work uses a detailed electrolyte model that builds on the DG model by quantifying the effect of salt concentration and salt molecular weight on RFB price. The DG model accounts for salt and solvent cost using an electrolyte cost per unit mass ($c_{m,e\pm}$ in units of \$ kg^{-1}). By lumping salt and solvent costs together in this manner, the DG model did not capture the sensitivity of battery price to salt concentration and molecular weight. Thus, the present detailed electrolyte model expands the electrolyte cost per unit mass in terms of the mass ratio of salt to total mass of salt and solvent S_{salt}, as well as the costs per unit mass of the salt and solvent (c_{salt} and $c_{solvent}$, respectively):

$$c_{m,e} = S_{salt}c_{salt} + (1 - S_{salt})c_{solvent} \tag{A1}$$

To capture salt and solvent costs explicitly, the electrolyte cost per unit mass for each electrolyte ($c_{m,e+}$ and $c_{m,e-}$) was substituted into the battery price expression from Ref. [9]. The resulting expression for battery price expressed in terms of the average molar salt ratio r_{avg} and the average redox-active species concentration b_{avg}. In terms of parameters from the DG model, r_{avg} and b_{avg} are expressed as:

$$r_{avg} = \frac{1}{2}\left(\frac{s_+M_+S_{salt+}}{\chi_+ n_{e+}M_{salt+}S_+} + \frac{s_-M_-S_{salt-}}{\chi_- n_{e-}M_{salt-}S_-}\right), \tag{A2}$$

$$\frac{1}{b_{avg}} = \frac{1}{2}\left[\frac{s_+M_+(1 - S_{salt+})}{\chi_+ n_{e+}S_+} + \frac{s_-M_-(1 - S_{salt-})}{\chi_- n_{e-}S_-}\right], \tag{A3}$$

where the redox-active species concentration S is expressed in units of kilograms per kilogram of solvent.

List of symbols

$b_{\pm}$	individual electrolyte active species molality, mol kg^{-1}
b_{avg}	mean active species molality, mol kg^{-1}
c_a	reactor cost per unit area, \$ m^{-2}
c_{add}	addition to price, \$ kW^{-1}
c_{bop}	balance-of-plant cost, \$ kW^{-1}
$c_{m,\pm}$	active material cost per unit mass, \$ kg^{-1}
$c_{me,\pm}$	electrolyte cost per unit mass, \$ kg^{-1}
c_{salt}	salt cost per unit mass, \$ kg^{-1}
$c_{solvent}$	solvent cost per unit mass, \$ kg^{-1}
$C_{Additional}$	additional cost, \$ kWh^{-1}
C_{BOP}	balance-of-plant cost, \$ kWh^{-1}
$C_{Electrolyte}$	electrolyte cost, \$ kWh^{-1}
$C_{Reactor}$	reactor cost, \$ kWh^{-1}
E_d	battery discharge energy, kWh
F	Faraday constant, kAh mol^{-1}
$M_{\pm}$	active species molecular weight, g mol^{-1}

M_{salt}	salt molecular weight, g mol^{-1}
$n_{e\pm}$	number of electrons stored per active molecule, mol$_{e^-}$ mol^{-1}
P_0	battery future-state price, $
$r_{\pm}$	individual electrolyte molar salt ratio, mol mol^{-1}
r_{avg}	mean molar salt ratio, mol mol^{-1}
R	area-specific resistance, Ω-cm^2
$s_{\pm}$	stoichiometric coefficient, mol mol^{-1}
$S_{\pm}$	active species solubility, kg kg^{-1}
$S_{salt,\pm}$	salt solubility, kg kg^{-1}
t_d	battery discharge time, h
U	open-circuit cell voltage, V
$\epsilon_{q,rt}$	round-trip coulombic efficiency
$\epsilon_{sys,d}$	system discharge efficiency
$\epsilon_{v,d}$	voltage discharge efficiency
$\chi_{\pm}$	depth-of-discharge

List of abbreviations

+	positive electrolyte
−	negative electrolyte
AM	active material
Aq	aqueous
ARPA-E	Advanced Research Projects Agency − Energy
ASR	area-specific resistance
BOP	balance-of-plant
Conc	concentration
DG	Darling and Gallagher et al.
DOE	Department of Energy
e	electron
NAq	nonaqueous
RFB	redox flow battery
SOC	state of charge
TE	techno-economic

Appendix A. Supplementary data

Supplementary data related to this article can be found at http://dx.doi.org/10.1016/j.jpowsour.2016.08.129.

References

[1] P. Denholm, E. Ela, B. Kirby, M. Milligan, The Role of Energy Storage with Renewable Electricity Generation: NREL/TP-6A2−47187, 2010.
[2] I. Gyuk, M. Johnson, J. Vetrano, K. Lynn, W. Parks, R. Handa, et al., Grid Energy Storage, US Department of Energy, Washington DC, 2013.
[3] U.S. Department of Energy, Office of Electricity Delivery and Energy Reliability, Energy Storage: Program Planning Document, 2011.
[4] C. Ponce de León, A. Frias-Ferrer, J. Gonzalez-Garcia, D.A. Szanto, F.C. Walsh, Redox flow cells for energy conversion, J. Power Sources 160 (2006) 716−732.
[5] P.K. Leung, X. Li, C. Ponce de León, L. Berlouis, C.T.J. Low, F.C. Walsh, Progress in redox flow batteries, remaining challenges and their applications in energy storage, RSC Adv. 2 (2012) 10125−10156.
[6] M. Skyllas-Kazacos, M.H. Chakrabarti, S.A. Hajimolana, F.S. Mjalli, M. Saleem, Progress in flow battery research and development, J. Electrochem. Soc. 158 (2011) R55.
[7] A.Z. Weber, M.M. Mench, J.P. Meyers, P.N. Ross, J.T. Gostick, Q. Liu, Redox flow batteries: a review, J. Appl. Electrochem 41 (2011) 1137−1164.
[8] W. Wang, Q. Luo, B. Li, X. Wei, L. Li, Z. Yang, Recent progress in redox flow battery research and development, Adv. Funct. Mater. 23 (2013) 970−986.
[9] R.M. Darling, K.G. Gallagher, J.A. Kowalski, S. Ha, F.R. Brushett, Pathways to low-cost electrochemical energy storage: a comparison of aqueous and nonaqueous flow batteries, Energy Environ. Sci. 7 (2014) 3459−3477.
[10] V. Viswanathan, A. Crawford, D. Stephenson, S. Kim, W. Wang, B. Li, et al., Cost and performance model for redox flow batteries, J. Power Sources 247 (2014) 1040−1051.
[11] S. Ha, K.G. Gallagher, Estimating the system price of redox flow batteries for grid storage, J. Power Sources 296 (2015) 122−132.
[12] U. S. Department of Energy, Headquarters Advanced Research Projects Agency − Energy (ARPA-E), Grid-Scale Rampable Intermittent Dispatchable Storage Funding Opportunity Announcement, 2010.
[13] P. Alotto, M. Guarnieri, F. Moro, Redox flow batteries for the storage of renewable energy: a review, Renew. Sustain. Energy Rev. 29 (2014) 325−335.
[14] J. Goeltz, D. Amadeo, A.J. Esswein, T.D. Jarvi, E.R. King, S.Y. Reece, et al., Aqueous Redox Flow Batteries Comprising Metal Ligand Coordination Compounds, 2014. US 2014/0028260 A1.
[15] Z. Yang, J. Zhang, M.C.W. Kintner-Meyer, X. Lu, D. Choi, J.P. Lemmon, et al., Electrochemical energy storage for green grid, Chem. Rev. 111 (2011) 3577−3613.
[16] Y. Matsuda, K. Tanaka, M. Okada, U. Takasu, M. Morita, A rechargeable redox battery utilizing ruthenium complexes with non-aqueous organic electrolyte, J. Appl. Electrochem. 18 (1988) 909−914.
[17] M.H. Chakrabarti, R.A.W. Dryfe, E.P.L. Roberts, Evaluation of electrolytes for redox flow battery applications, Electrochim. Acta 52 (2007) 2189−2195.
[18] M.H. Chakrabarti, E.P. Lindfield Roberts, M. Saleem, Charge−discharge performance of a novel undivided redox flow battery for renewable energy storage, Int. J. Green Energy 7 (2010) 445−460.
[19] A.A. Shinkle, T.J. Pomaville, A.E.S. Sleightholme, L.T. Thompson, C.W. Monroe, Solvents and supporting electrolytes for vanadium acetylacetonate flow batteries, J. Power Sources 248 (2014) 1299−1305.
[20] X. Wei, G.G. Xia, B. Kirby, E. Thomsen, B. Li, Z. Nie, et al., An aqueous redox flow battery based on neutral alkali metal ferri/ferrocyanide and polysulfide electrolytes, J. Electrochem. Soc. 163 (2016) A5150−A5153.
[21] H. Pan, X. Wei, W.A. Henderson, Y. Shao, J. Chen, P. Bhattacharya, et al., On the way toward understanding solution chemistry of lithium polysulfides for high energy Li-S redox flow batteries, Adv. Energy Mater. 5 (2015) 150113.
[22] K. Lin, Q. Chen, M.R. Gerhardt, L. Tong, S.B. Kim, L. Eisenach, et al., Alkaline quinone flow battery, Science 80 (2015) 1529−1532, 349.
[23] B. Huskinson, M.P. Marshak, C. Suh, S. Er, M.R. Gerhardt, C.J. Galvin, et al., A metal-free organic-inorganic aqueous flow battery, Nature 505 (2014) 195−198.
[24] F.R. Brushett, J.T. Vaughey, A.N. Jansen, An all-organic non-aqueous lithium-ion redox flow battery, Adv. Energy Mater. 2 (2012) 1390−1396.
[25] S.H. Oh, C.W. Lee, D.H. Chun, J.D. Jeon, J. Shim, K.H. Shin, et al., A metal-free and all-organic redox flow battery with polythiophene as the electroactive species, J. Mater. Chem. A 2 (2014) 19994−19998.
[26] S.K. Park, J. Shim, J.H. Yang, K.H. Shin, C.S. Jin, B.S. Lee, et al., Electrochemical properties of a non-aqueous redox battery with all-organic redox couples, Electrochem. Commun. 59 (2015) 68−71.
[27] X. Wei, W. Xu, J. Huang, L. Zhang, E. Walter, C. Lawrence, et al., Radical compatibility with nonaqueous electrolytes and its impact on an all-organic redox flow battery, Angew. Chem. Int. Ed. 54 (2015) 8684−8687.
[28] X. Wei, W. Xu, M. Vijayakumar, L. Cosimbescu, T. Liu, V. Sprenkle, et al., TEMPO-based catholyte for high-energy density nonaqueous redox flow batteries, Adv. Mater. 26 (2014) 7649−7653.
[29] J.D. Milshtein, L. Su, C. Liou, A.F. Badel, F.R. Brushett, Voltammetry study of quinoxaline in aqueous electrolytes, Electrochim. Acta 180 (2015) 695−704.
[30] Y. Xu, Y.H. Wen, J. Cheng, G.P. Cao, Y.S. Yang, A study of tiron in aqueous solutions for redox flow battery application, Electrochim. Acta 55 (2010) 715−720.
[31] A.P. Kaur, N.E. Holubowitch, S. Ergun, C.F. Elliott, S.A. Odom, A highly soluble organic catholyte for non-aqueous redox flow batteries, Energy Technol. 3 (2015) 476−480.
[32] J. Huang, L. Cheng, R.S. Assary, P. Wang, Z. Xue, A.K. Burrell, et al., Liquid catholyte molecules for nonaqueous redox flow batteries, Adv. Energy Mater. 5 (2015) 1401782.
[33] J. Huang, L. Su, J.A. Kowalski, J.L. Barton, M. Ferrandon, A.K. Burrell, et al., A subtractive approach to molecular engineering of dimethoxybenzene-based redox materials for non-aqueous flow batteries, J. Mater. Chem. A 3 (2015) 14971−14976.
[34] T. Liu, X. Wei, Z. Nie, V. Sprenkle, W. Wang, A total organic aqueous redox flow battery employing a low cost and sustainable methyl viologen anolyte and 4-HO-TEMPO catholyte, Adv. Energy Mater. 6 (2016) 1501449.
[35] J.A. Kowalski, L. Su, J.D. Milshtein, F.R. Brushett, Recent advances in molecular engineering of redox active organic molecules for nonaqueous flow batteries, Curr. Opin. Chem. Eng 13 (2016) 45−52.
[36] K.G. Gallagher, S. Goebel, T. Greszler, M. Mathias, W. Oelerich, D. Eroglu, et al., Quantifying the promise of lithium−air batteries for electric vehicles, Energy Environ. Sci. 7 (2014) 1555.
[37] P.A. Nelson, K.G. Gallagher, I. Bloom, D.W. Dees, Modeling the Performance and Cost of Lithium-ion Batteries for Electric-Drive Vehicles, 2012.
[38] C. Zhou, K. Qian, M. Allan, W. Zhou, Modeling of the cost of EV battery wear due to V2G application in power systems, IEEE Trans. Energy Convers. 26 (2011) 1041−1050.
[39] G. Kear, A.A. Shah, F.C. Walsh, Development of the all-vanadium redox flow battery for energy storage: a review of technological, financial and policy aspects, Int. J. Energy Res. 36 (2012) 1105−1120.
[40] M. Zhang, M. Moore, J.S. Watson, T.A. Zawodzinski, R.M. Counce, Capital cost sensitivity analysis of an all-vanadium redox-flow battery, J. Electrochem. Soc. 159 (2012) A1183−A1188.
[41] R. Darling, K. Gallagher, W. Xie, L. Su, F. Brushett, Transport property requirements for flow battery separators, J. Electrochem. Soc. 163 (2016) A5029−A5040.
[42] D. Rastler, Electric Power Research Institute, Market Driven Distributed Energy Storage System Requirements for Load Management Applications, 2007.
[43] ICIS Indicative Chemical Prices A-Z, Indicative Chemical Prices A-Z, 2006. http://www.icis.com/chemicals/channel-info-chemicals-a-z/.
[44] L. Gaines, R. Cuenca, Costs of Lithium-Ion Batteries for Vehicles, 2000.

[45] B. Yang, L. Hoober-Burkhardt, F. Wang, G.K. Surya Prakash, S.R. Narayanan, An inexpensive aqueous flow battery for large-scale electrical energy storage based on water-soluble organic redox couples, J. Electrochem. Soc. 161 (2014) A1371–A1380.
[46] R.A. Potash, J.R. McKone, S. Conte, H.D. Abruña, On the benefits of a symmetric redox flow battery, J. Electrochem. Soc. 163 (2016) A338–A344.
[47] A.J. Cofrancesco, Anthraquinone, in: Kirk-Othmer Encycl. Chem. Technol. Anthraquinone, John Wiley & Sons, Inc., New York, 2001, pp. 1–13.
[48] F.Y. Fan, W.H. Woodford, Z. Li, N. Baram, K.C. Smith, A. Helal, et al., Polysulfide flow batteries enabled by percolating nanoscale conductor networks, Nano Lett. 14 (2014) 2210–2218.
[49] S.H. Shin, S.H. Yun, S.H. Moon, A review of current developments in non-aqueous redox flow batteries: characterization of their membranes for design perspective, RSC Adv. 3 (2013) 9095.
[50] D. Pletcher, R. Wills, A novel flow battery: a lead acid battery based on an electrolyte with soluble lead(II) Part II. Flow cell studies, Phys. Chem. Chem. Phys. 6 (2004) 1779–1785.
[51] D. Aurbach, Y. Talyosef, B. Markovsky, E. Markevich, E. Zinigrad, L. Asraf, et al., Design of electrolyte solutions for Li and Li-ion batteries: a review, Electrochim. Acta 50 (2004) 247–254.
[52] J. Mun, M.-J. Lee, J.-W. Park, D.-J. Oh, D.-Y. Lee, S.-G. Doo, Non-aqueous redox flow batteries with nickel and iron tris(2,2′-bipyridine) complex electrolyte, Electrochem. Solid-State Lett. 15 (2012) A80–A82.
[53] I.L. Escalante-García, J.S. Wainright, L.T. Thompson, R.F. Savinell, Performance of a non-aqueous vanadium acetylacetonate prototype redox flow battery: examination of separators and capacity decay, J. Electrochem. Soc. 162 (2015) A363–A372.
[54] C.S. Sevov, R.E.M. Brooner, E. Chénard, R.S. Assary, J.S. Moore, J. Rodríguez-López, et al., Evolutionary design of low molecular weight organic anolyte materials for applications in nonaqueous redox flow batteries, J. Am. Chem. Soc. 137 (2015) 14465–14472.
[55] R. Younesi, G.M. Veith, P. Johansson, K. Edstrom, T. Vegge, Lithium salts for advanced lithium batteries: Li-metal, Li-O2, and Li-S, Energy Environ. Sci. 8 (2015) 1905–1922.
[56] K. Xu, Electrolytes and interphases in Li-Ion batteries and beyond, Chem. Rev. 114 (2014) 11503–11618.
[57] S.M. Laramie, J.D. Milshtein, T.M. Breault, F.R. Brushett, L.T. Thompson, Performance and cost characteristics of multi-electron transfer, common ion exchange non-aqueous redox flow batteries, J. Power Sources 327 (2016) 681–692.
[58] B. Scrosati, Lithium rocking chair batteries: an old concept? J. Electrochem. Soc. 139 (1992) 2776.
[59] N.S. Hudak, L.J. Small, H.D. Pratt, T.M. Anderson, Through-plane conductivities of membranes for nonaqueous redox flow batteries, J. Electrochem. Soc. 162 (2015) A2188–A2194.
[60] P.J. Cabrera, X. Yang, J.A. Suttil, K.L. Hawthorne, R.E.M. Brooner, M.S. Sanford, et al., Complexes containing redox noninnocent ligands for symmetric, multielectron transfer nonaqueous redox flow batteries, J. Phys. Chem. C 119 (2015) 15882–15889.
[61] J.H. Kim, K.J. Kim, M.S. Park, N.J. Lee, U. Hwang, H. Kim, et al., Development of metal-based electrodes for non-aqueous redox flow batteries, Electrochem. Commun. 13 (2011) 997–1000.
[62] J. Mun, M.J. Lee, J.W. Park, D.J. Oh, D.Y. Lee, S.G. Doo, Non-aqueous redox flow batteries with nickel and iron tris (2, 2′-bipyridine) complex electrolyte, Electrochem. Solid-State Lett. 15 (2012) A80–A82.
[63] L. Su, R.M. Darling, K.G. Gallagher, W. Xie, J.L. Thelen, A.F. Badel, et al., An investigation of the ionic conductivity and species crossover of lithiated nafion N117 in nonaqueous electrolytes, J. Electrochem. Soc. 163 (2016) A5253–A5262.
[64] S.H. Shin, Y. Kim, S.H. Yun, S. Maurya, S.H. Moon, Influence of membrane structure on the operating current densities of non-aqueous redox flow batteries: organic–inorganic composite membranes based on a semi-interpenetrating polymer network, J. Power Sources 296 (2015) 245–254.
[65] L. Su, M. Ferrandon, J.A. Kowalski, J.T. Vaughey, F.R. Brushett, Electrolyte development for non-aqueous redox flow batteries using a high-throughput screening platform, J. Electrochem. Soc. 161 (2014) A1905–A1914.
[66] J.D. Milshtein, J.L. Barton, R.M. Darling, F.R. Brushett, 4-acetamido-2,2,6,6-tetramethylpiperidine-1-oxyl as a model organic redox active compound for nonaqueous redox flow batteries, J. Power Sources 327 (2016) 151–159.
[67] M.A. Miller, J.S. Wainright, R.F. Savinell, Communication—Iron ionic liquid electrolytes for redox flow battery applications, J. Electrochem. Soc. 163 (2016) A578–A579.
[68] L. Bahadori, M.A. Hashim, N.S.A. Manan, F.S. Mjalli, I.M. AlNashef, N.P. Brandon, et al., Investigation of ammonium- and phosphonium-based deep eutectic solvents as electrolytes for a non-aqueous all-vanadium redox cell, J. Electrochem. Soc. 163 (2016) A632–A638.
[69] N.V. Plechkova, K.R. Seddon, Applications of ionic liquids in the chemical industry, Chem. Soc. Rev. 37 (2008) 123–150.
[70] L. Chen, M. Sharifzadeh, N. Mac Dowell, T. Welton, N. Shah, J.P. Hallett, Inexpensive ionic liquids: [HSO4]−-based solvent production at bulk scale, Green Chem. 16 (2014) 3098.
[71] J. Luo, J. Hu, W. Saak, R. Beckhaus, G. Wittstock, I.F.J. Vankelecom, et al., Protic ionic liquid and ionic melts prepared from methanesulfonic acid and 1H-1,2,4-triazole as high temperature PEMFC electrolytes, J. Mater. Chem. 21 (2011) 10426–10436.
[72] L. Hu, Z. Xue, K. Amine, Z. Zhang, Fluorinated electrolytes for 5-V Li-Ion chemistry: synthesis and evaluation of an additive for high-voltage LiNi0. 5Mn1. 5O4/Graphite cell, J. Electrochem. Soc. 161 (2014) A1777–A1781.
[73] Z. Chen, J. Liu, A.N. Jansen, G. GirishKumar, B. Casteel, K. Amine, Lithium borate cluster salts as redox shuttles for overcharge protection of lithium-ion cells, Electrochem. Solid-State Lett. 13 (2010) A39.
[74] T. Janoschka, N. Martin, U. Martin, C. Friebe, S. Morgenstern, H. Hiller, et al., An aqueous, polymer-based redox-flow battery using non-corrosive, safe, and low-cost materials, Nature 527 (2015) 78–81.
[75] N.G. Connelly, W.E. Geiger, Chemical redox agents for organometallic chemistry, Chem. Rev. 96 (1996) 877–910.
[76] Y. Liang, Z. Tao, J. Chen, Organic electrode materials for rechargeable lithium batteries, Adv. Energy Mater. 2 (2012) 742–769.
[77] Z. Song, H. Zhou, Towards sustainable and versatile energy storage devices: an overview of organic electrode materials, Energy Environ. Sci. 6 (2013) 2280–2301.
[78] R.T. Boeré, T.L. Roemmele, Electrochemistry of redox-active Group 15/16 heterocyles, Coord. Chem. Rev. 210 (2000) 369–445.
[79] A. Jain, S.P. Ong, G. Hautier, W. Chen, W.D. Richards, S. Dacek, et al., The Materials Project: a materials genome approach to accelerating materials innovation, Apl. Mater 1 (2013) 11002.
[80] RFB Dashboard, The Materials Project, 2016. https://materialsproject.org/#apps/RFBDashboard.